Vol. 03, Iss. 4 (2025) 470-482, DOI: 10.61552/JME.2025.04.012

JME

Journal of Materials and Engineering

www.jme.aspur.rs

Research article

A Facile and Cost-Effective Synthesis of Manganese Carbonate and Manganese Dioxide from Bajaur Manganese Ore

Waheed Ur Rehman[a,*], Amin Ur Rehman[a], Asma Yamin[a]

[a]*PCSIR Laboratories Complex, Jamrud Road, Peshawar-25120, Pakistan.*

Keywords:

Manganese carbonate
Manganese dioxide
Rhodochrosite
Extractant
Precipitant
Calcination

* Corresponding author:

Waheed Ur Rehman
E-mail: contactwaheed@hotmail.com

Received: 20 November 2024
Revised: 26 December 2024
Accepted: 30 January 2025

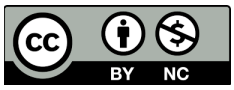

A B S T R A C T

In the present study, manganese ore of district Bajaur, Pakistan, was evaluated for the synthesis of manganese carbonate ($MnCO_3$) through a facile and cost-effective approach, employing hydrochloric acid (HCl) as an extractant, and soda ash (Na_2CO_3) as a precipitant at different temperatures and times. The optimum yield and maximum manganese content in the prepared $MnCO_3$ was found to be 78.10% and 28.54%, respectively, at a temperature of 70°C and a time of 3 hours. $MnCO_3$ was then calcined to manganese dioxide (MnO_2) at elevated temperatures. SEM-EDX, XRD, and FTIR techniques were applied to explore the morphology, crystal structure, and purity of the developed products. The major mineral phase in $MnCO_3$ was rhodochrosite having a cubical morphology. An increase in calcination temperature from 500 to 900°C, progressively changed MnO_2 from α-MnO_2 to β-MnO_2 polymorph. A flowsheet has also been proposed for the commercial production of the two products.

1. INTRODUCTION

Almost 90% of the globally produced manganese metal is consumed as a deoxidizer, desulfuriser, and alloying agent in steel manufacturing. The remaining 10% is deployed in non-metallurgical applications like batteries (dry cell and lithium ion), chemicals, fertilizers, electrode materials, magnetic materials, foods, pharmaceuticals, catalysts, aluminium alloys, animal feed etc. [1-3]. Such a huge applications make manganese the fourth most used metal after iron, aluminium, and copper. As per the report of U.S. Geological Survey, the global reserves of manganese are estimated to be 690 million tons on metal basis. A giant share of 70% of the world's total manganese is contributed by South Africa, while the rest comes from Australia, China, Gabon, Brazil, Ukraine, India, Ghana, Kazakhstan, and Mexico. Manganese in the native ores mainly

occur either as carbonates, oxides, and silicates. Around 40% of the manganese ores are dominated by carbonate minerals, 25% by silicate minerals, and 20% by oxide minerals. According to purity, manganese ores are categorized as high, medium, and low grade, which contain 44–48% Mn, 35–44% Mn, and 25–35% Mn, respectively [4-7].

Manganese carbonate ($MnCO_3$) finds extensive uses in the production of ferrites, alloys, ceramic glazes, welding electrodes, paints, fertilizers, dietaries, solid oxide fuel cells, and as precursor for the production many chemical compounds [8, 9]. Lu et. Al. prepared spherical manganese $MnCO_3$ templates by using $MnSO_4.H_2O$ and $NaHCO_3$ as precursors in a facile chemical precipitation technique. An excellent photocatalytic performance was exhibited by the $MnCO_3$ template [10]. Zhang and Jia synthesized $MnCO_3$ nanowires and microcubes through an ethylene glycol mediated solution method and investigated their adsorption properties towards fluoride. The adsorption capacities of the nanowires were found to be higher than that of the microtubes [11]. Reyes et. al. thermally analyzed rhodochrosite ore at calcination temperatures of 100 to 1200°C. The three consecutive mass losses were ascribed to the transformation from carbonate to manganese (III) oxide, the reduction to manganese tetroxide, and the decomposition of $CaCO_3$, respectively [12]. Yannick et. al. carried out the precipitation tests on a sample of the cobalt removal solution containing manganese as an impurity. Na_2CO_3 was used as a precipitating agent forming $MnCO_3$ precipitates, which were further calcined to MnO_2 at temperatures of 370, 420, and 470˚C. A precipitation yield and manganese content of 98.43% and 24.21%, respectively were obtained in one hour at 25˚C, and a pH of 8.5. A highest loss in mass was observed at 470˚C after 4 hours of calcination [13]. Muralikrishna et. al. studied the properties of hierarchical superstructures of $MnCO_3$ and $MnCO_3$–reduced graphene oxide hybrid nanocomposites with cubical, spherical, dumbbell, and oval crystal structures, using green tree extract as a reducing agent and shape controlling agent. The composite material showed good performance in lithium-ion batteries as an anode material [14].

The major polymorphs of manganese dioxide (MnO_2) are α, β, γ, and δ-MnO_2. A lot of research is underway to explore their potential applications in catalysis, batteries, oxidation processes, and ion exchange, etc. [15]. Srither et. al. prepared MnO_2 nanoparticles by spray pyrolysis technique using manganese nitrate solution as a metal precursor. The results revealed that the MnO_2 nanoparticles thus produced could be effectively used as an electrode material for supercapacitors [16]. Wang et. al. employed hydrothermally prepared MnO_2 nanotubes, nanowires, nanocubes, and nanoflowers as a catalyst for toluene conversion, using $KMnO_4$ and $MnSO_4$ as precursors. Highest activity was shown by MnO_2 towards toluene, due to a large surface area and Mn^{4+} content [17]. A mild hydrothermal route was adopted by Khan et. al. to synthesize urchin-like γ-MnO_2 nanostructures subsequently transforming to α-MnO_2 nanowires, by directly reacting $MnSO_4$ and $KClO_3$. Reaction time was found to be helpful in controlling various crystalline forms of MnO_2 [18]. Similarly, Feng et. al. developed urchin and caddice-clew-like crystal morphologies of α-MnO_2, using a hydrothermal route. Urchin-like α-MnO_2 crystals showed better electrochemical performance in lithium-ion battery [19]. Wang et.al. attempted to reduce the fire hazards of epoxy composites by employing various crystalline forms and morphologies of MnO_2 nanoparticles. The thermal stability of the composites was enhanced by using α-nanosheets, as compared to α-nanospheres and β-nanorods [20]. Rus et. al. studied the electrochemical behaviour of γ-MnO_2 in KOH and LiOH solutions. It was observed that the cyclability of γ-MnO_2 was better in a combination of both solutions as compared to the use of independent solutions [21]. Chen et. al. synthesized MnO_2 nanorods through a simple hydrothermal method using $KMnO_4$ and HCl as precursors. A significant enhancement in the electrochemical performance of MnO_2 nanorods was demonstrated which was mainly attributed to the unique structure of MnO_2 nanorods and the use of CMC binder [22]. Sannasi and Subbian applied a facile microwave method to prepare α, and β-MnO_2 from natural moringa oleifera gum. The prepared materials were shown to be appropriate for pseudo-capacitor applications [23].

In Pakistan, there are a few deposits of manganese. Important reserves in the south are in Lasbela, Siro (Karachi), Snjro Dhora (Kallat), Khabri and Dadi Dhora. These deposits constitute ~97% of the country's total reserves. Other deposits which occur in north are in Hazara and

Nushki. The total reserves of manganese in Pakistan worked out so far are estimated to be 0.5 million tons, and the annual production varies from 100 to 600 tons. Moreover, 0.120 million tons of manganese ore reserves have been identified in Bajaur and Mohmand districts [24-26]. Although the beneficiation studies have been carried out on these reserves [27-29], nevertheless, to the best of our knowledge, these have not yet been tested in the preparation of value-added products like $MnCO_3$ and MnO_2.

In the present study, we have attempted to synthesize $MnCO_3$ from the native ore of district Bajaur, Pakistan. Hydrochloric Acid (HCl) was used as an extractant, which has scarcely been applied before. The synthesized $MnCO_3$ was then calcined to MnO_2 at various temperatures. $MnCO_3$ and MnO_2 were evaluated in detail for their morphology and crystalline forms. It is also worth mentioning that the manganese ore was used without any beneficiation process. Therefore, the use of cheap HCl as an extractant and elimination of beneficiation process makes the process more economical. The two products thus prepared can be further tested and applied in various potential areas as discussed in the previous paras. A flowsheet has also been proposed for the commercial production of these products as per the developed process. The study is expected to lay a foundation for the gainful utilization of huge manganese deposits reserved in the area.

2. MATERIALS & METHODS

Manganese ore of district Bajaur, Pakistan was used as a starting raw material. Hydrochloric acid (HCl) of Sitara Chemicals, Pakistan, and Soda ash (Na_2CO_3) of Imperial Chemical Industries, Pakistan were used in the synthesis of $MnCO_3$ and MnO_2. Both the chemicals used were of commercial grade.

2.1 Synthesis of $MnCO_3$ and MnO_2 from Manganese Ore

Manganese ore was first crushed in a blake type jaw crusher to reduce its size to ½ - 1″. A fine particle size of -200 mesh was achieved by grinding the crushed ore in a rod mill. 500 gm of manganese powder was then reacted with an acidic solution comprising of 1370 ml of 33% HCl and 1000 ml of water, under mechanical stirring in a double jacket glass reactor having a total capacity of 20 liter. Three reactions were run at a temperature of 50, 70, and 90°C. At each temperature, the reaction was run for 3, 6, and 9 hours to evaluate the conversion to $MnCl_2$. After completion of each reaction time, the $MnCl_2$ solution was drained in a polyethylene container. All the solutions were filtered through a vacuum filter to obtain a clear filtrate. Precipitation reactions were then carried out by slowly adding Na_2CO_3 to the $MnCl_2$ solutions under continuous stirring, until the solutions were neutralized. Each of the precipitated $MnCO_3$ was filtered through a vacuum filter to obtain a moist filter cake, which was finally dried in a vacuum oven at 80°C to obtain dry $MnCO_3$ powder.

The interactions between hydrochloric acid (HCl) and the various components present in the raw manganese ore, including SiO_2, Fe, $Mg(CO_3)_2$, and MnO_2 can be explained as following.

Silicon dioxide (SiO_2) is generally resistant to attack by HCl under normal conditions. SiO_2 is a highly stable compound with strong Si-O bonds, and HCl does not react with it at room temperature or even under mildly elevated temperatures typically used in our experiments. Thus, SiO_2 remains largely inert in the presence of HCl, which explains its persistence as a solid impurity in many mineral processing scenarios. This inert behaviour aligns with our observation that SiO_2 was effectively removed in the $MnCO_3$ synthesis, likely through mechanical separation rather than chemical reaction.

Iron in the ore could exist in various oxidation states, typically as Fe^{2+} or Fe^{3+} compounds such as iron oxides (Fe_2O_3 or Fe_3O_4). In the presence of HCl, iron oxides react to form soluble iron chloride ($FeCl_2$ or $FeCl_3$) according to the following reactions:

$$Fe_2O_3 + 6HCl \rightarrow 2FeCl_3 + 3H_2O \quad (1)$$

$$Fe_3O_4 + 8HCl \rightarrow FeCl_2 + 2FeCl_3 + 4H_2O \quad (2)$$

Magnesium carbonate ($MgCO_3$) reacts with HCl to produce soluble magnesium chloride ($MgCl_2$), carbon dioxide, and water:

$$MgCO_3 + 2HCl \rightarrow MgCl_2 + CO_2 + H_2O \quad (3)$$

Given the solubility of $MgCl_2$ in water, magnesium is effectively removed from the solid phase, contributing to the purification of the $MnCO_3$. The reduction in Mg content observed in the synthesized $MnCO_3$ is consistent with this reaction pathway.

Manganese dioxide (MnO_2) can react with HCl in a redox reaction, where MnO_2 is reduced to $MnCl_2$, and HCl is oxidized to chlorine gas (Cl_2):

$$MnO_2 + 4HCl \rightarrow MnCl_2 + Cl_2 + 2H_2O \quad (4)$$

This reaction reduces MnO_2 to the more soluble $MnCl_2$, which can be further processed to form $MnCO_3$ during the hydrothermal treatment. The conversion of MnO_2 to $MnCl_2$ in the presence of HCl is an essential step in the extraction of manganese from the ore.

The reaction between $MnCl_2$ and Na_2CO_3 proceeds as following,

$$MnCl_{2(aq)} + Na_2CO_{3(s)} \rightarrow MnCO_3 + 2NaCl \quad (5)$$

The dry $MnCO_3$ powder was subjected to calcination temperatures of 500, 700, and 900°C in a laboratory muffle furnace, for a period of 1 hour each. The calcination reaction for conversion of $MnCO_3$ can be presented as [30],

$$2MnCO_3 + O_2 \xrightarrow{\Delta} 2MnO_2 + 2CO_2 \quad (6)$$

The calcined samples were carefully collected in polythene sample bags. Both $MnCO_3$ and MnO_2 samples were then subjected to various characterization techniques.

To determine the manganese content in manganese carbonate ($MnCO_3$) based on its purity and yield, the theoretical manganese content was first calculated, which was 47.79%, based on the molar masses of its constituents. This percentage represented manganese in pure $MnCO_3$. Next, the purity was considered, indicating the proportion of $MnCO_3$ in the final product, along with the yield, reflecting the efficiency of the synthesis process. The actual manganese content was obtained by multiplying the theoretical content by both the purity and yield, expressed as percentage. This method provided an accurate assessment of the manganese content, considering both impurities and process efficiency.

2.2 Characterization of $MnCO_3$ and MnO_2

To confirm the presence or absence of heavy metals, Atomic Absorption Spectrometer Hitachi Z 8000 Japan, was used to analyse the raw manganese ore sample. Lead was found to be less than 0.1 ppm, chromium less than 0.04 ppm, and cadmium less than 0.01 ppm, which are far below the hazardous level. The mineral phases in raw manganese ore, $MnCO_3$, and MnO_2 were determined through XRD, model JDX-3532, JEOL, Tokyo, Japan. The surface morphology and elemental composition of raw manganese ore, $MnCO_3$, and MnO_2 were studied through Scanning Electron Microscope (JSM6380, JEOL, Japan) accompanied with Energy Dispersive X-Ray (EDX) analyser. The instrument was operated at 20.0 kV and probe current of 1.0 nA with counting rate of 197-242 counts per second. The main functional groups were identified through FTIR, model PerkinElmer Spectrum 2/UATR, 103385 USA.

3. RESULTS & DISCUSSION

The X-ray diffraction (XRD) analysis shown in Figure 1 provides essential insights into the mineralogical composition of both the raw manganese ore and the synthesized $MnCO_3$. In the raw manganese ore, pyrolusite (MnO_2) is identified as the dominant mineral phase, prominently appearing at a 2-theta angle of approximately 65°, and also at 29° and 55°, consistent with the reference pattern PDF#00-044-0141 [31].

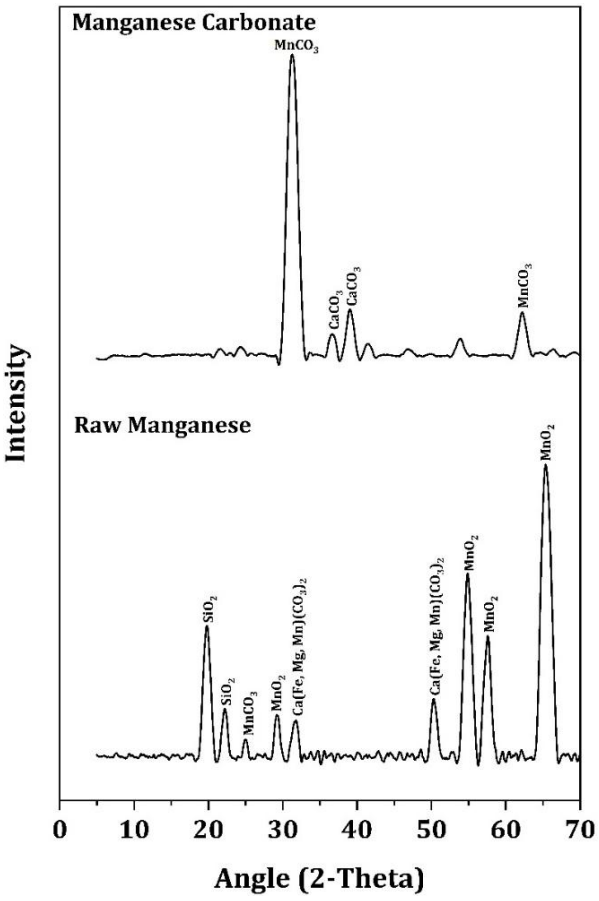

Fig. 1. XRD Analysis of Raw Manganese Ore & Manganese Carbonate.

Alongside pyrolusite, the raw ore contains additional mineral phases including ankerite, rhodochrosite, and quartz. Ankerite, a complex carbonate mineral with the formula Ca(Fe, Mg, Mn)$(CO_3)_2$, is identified through its characteristic peaks, as supported by multiple studies [1, 32-34]. Quartz, a prevalent gangue mineral, is also detected through its distinct sharp peaks, matching well with established diffraction data [7, 32, 35]. The presence of these mineral phases highlights the complex and heterogeneous nature of the raw manganese ore, underscoring the challenges associated with its purification. The identification of ankerite, rhodochrosite, and quartz alongside pyrolusite reveals a complicated mineral matrix that must be carefully managed during the extraction and synthesis processes to effectively isolate manganese carbonate. Understanding these mineralogical complexities is critical for developing optimized purification strategies and improving the overall efficiency of the manganese extraction process.

Upon synthesizing $MnCO_3$, the XRD diffractogram demonstrates a significant reduction in impurity peaks, indicating the effectiveness of the extraction and synthesis process. The synthesized $MnCO_3$ exhibits strong peaks at 2-θ angles of 31.14, 41.32, and 62.34, which are consistent with the hexagonal crystalline form of rhodochrosite. These peaks correspond to the lattice planes of $MnCO_3$, as per the ICDD-PDF 96-900-7692 standard [12]. This demonstrates that the process successfully isolated $MnCO_3$ from other manganese and non-manganese bearing minerals, achieving a high degree of phase purity. The hexagonal structure of rhodochrosite is a desirable form for various applications, indicating that the synthesized product is structurally well-defined. However, despite the high purity of the synthesized $MnCO_3$, the presence of minor impurities such as calcite and gibbsite are noted. These are observed as minor peaks in the diffractogram, suggesting that while the major impurities have been largely removed, complete purification was not achieved. The persistence of these minor phases could be attributed to incomplete reactions or the presence of finely intergrown minerals that are difficult to separate. The identification of calcite and gibbsite as residual impurities aligns with previous studies [12, 36-39], which often report the difficulty in fully eliminating such phases due to their chemical similarity to target minerals or their fine-grained nature.

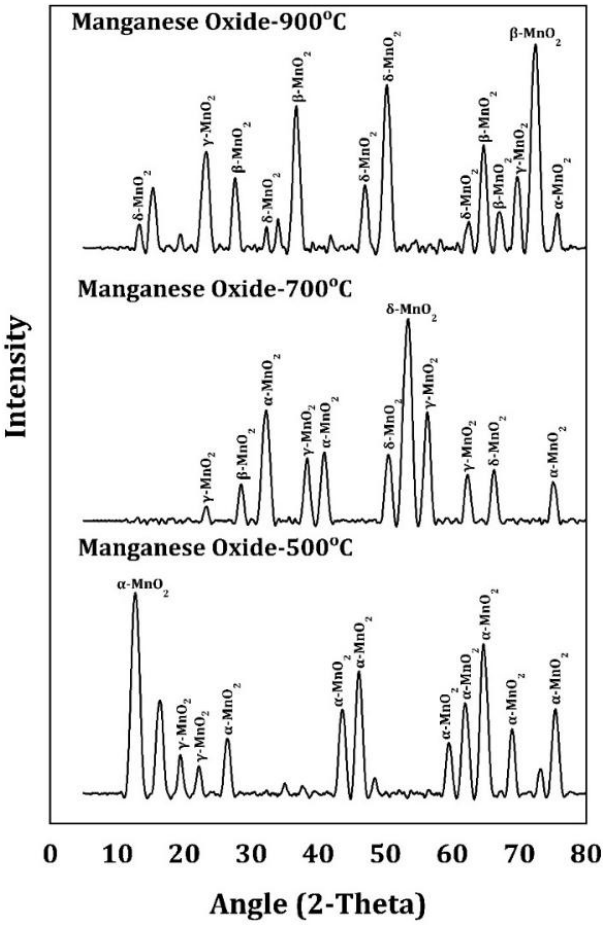

Fig. 2. XRD Analysis of (A) MnO_2 at 500°C (B) MnO_2 at 700°C (C) MnO_2 at 900°C.

Figure 2 shows the XRD diffractograms of MnO_2 formed at three different temperatures of 500, 700, and 900°C, respectively. It can be deduced that various MnO_2 polymorphs are formed at each temperature. At a temperature of 500°C, the major peaks observed are of α-MnO_2 [15, 17, 31, 40] which are accompanied by minor peaks of γ-MnO_2 [40]. At a temperature of 700°C, the major peaks observed are of δ-MnO2 [31, 40]. Moreover, α-MnO_2 [15, 40] and γ-MnO_2 [31, 40] polymorphs also contribute a good portion of the product at 700°C. At a temperature of 900°C, β-MnO2 [15, 17, 40] occurs as a major polymorph, followed by δ-MnO2 [31, 40] and γ-MnO_2 [40] polymorphs. The XRD spectra of α-MnO_2, β-MnO_2, γ-MnO_2, and δ-MnO_2 are consistent with the reference patterns JCPDS No. 44-141, JCPDS No. 24-0735, JCPDS No. 44-142, and JCPDS No. 43-1456, respectively [41]. So, it can be safely presumed that as the calcination temperature increases from 500 to 900°C, the MnO_2 progressively changes from α-MnO_2 to β-MnO2 polymorph. However, at each temperature, a mixture of various polymorphs exists, with one crystalline form dominating over the others.

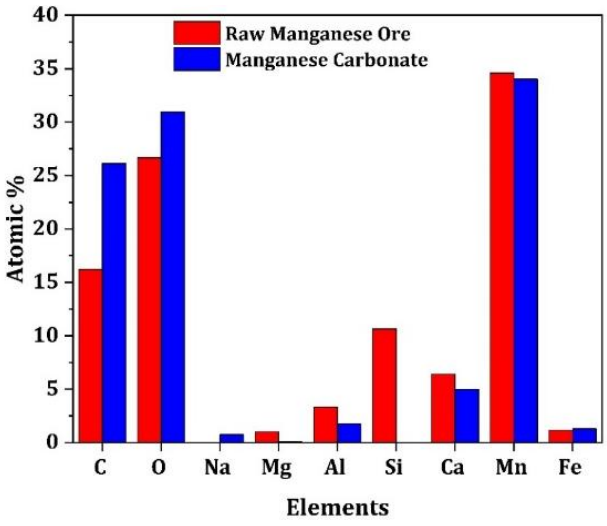

Fig. 3. Atomic% of Elements in Raw Manganese Ore & Manganese Carbonate.

Figure 3 shows the elemental analysis of raw manganese ore and $MnCO_3$. The bar graph depicts that manganese content in the raw ore remained almost unchanged (34%) in the synthesized $MnCO_3$. The carbon and oxygen percentages, however, increased in the synthesized $MnCO_3$ from 16% to 26%, and 27% to 31%, respectively. This improvement is an indication of the increase of $MnCO_3$ content in the hydrothermally treated ore. Similarly, the silicon percentage decreased from 11% in the raw rhodochrosite ore to 0% in the synthesized $MnCO_3$, which proves the complete removal of SiO_2 impurity. Other impurities such as magnesium, calcium and aluminium were also reduced significantly in the synthesized $MnCO_3$. It can be further observed that a small percentage of 0.75% of sodium appeared in the synthesized $MnCO_3$, which is most probably due the left-over sodium chloride in the product.

Figure 4 shows the elemental analysis of MnO_2 obtained at 500, 700, and 900°C, respectively. The bar graph shows a clear increase in the manganese content from 34% in the raw rhodochrosite ore to 52%, 55%, and 65.5% in the MnO_2 produced at 500°C, 700°C, and 900°C, respectively. The carbon content in the MnO_2 progressively reduced from 12.3% at 500°C to 0% at 900°C, which proves the successful conversion of $MnCO_3$ to MnO_2 at 900°C. However, the percentage of calcium increased from 7% at 500°C to 9% at 900°C, which depicts that calcium could not be removed at higher temperatures and it remained in the form of calcium oxide impurity in the final product. Other minor impurities, which remained intact in the product at 900°C, were aluminium and iron. The fate of calcium and iron during the experiments indicates that while some impurities can be reduced during initial hydrothermal treatment, the calcination process at higher temperatures may lead to the persistence or even reappearance of certain impurities, such as calcium in the form of calcium oxide, and iron, likely as iron oxide. This highlights the need for further optimization of the process conditions or additional purification steps to achieve higher purity in the final MnO_2 product.

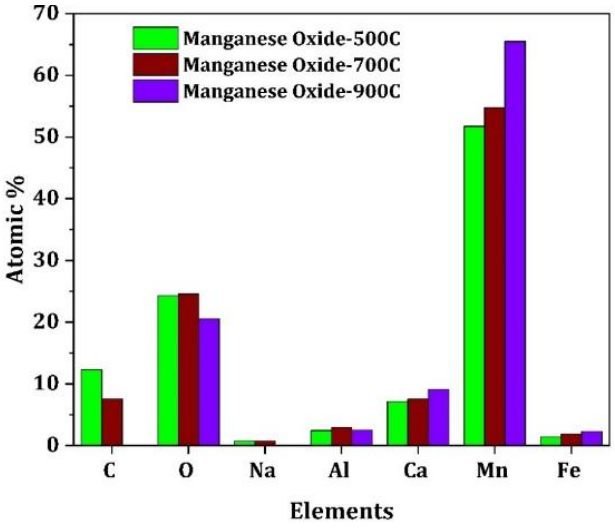

Fig. 4. Atomic% of Elements in (A) MnO_2 at 500°C (B) MnO_2 at 700°C (C) MnO2 at 900°C.

Figure 5 shows the SEM analysis of raw manganese ore and manganese carbonate at low and high magnifications. The original ore has a random morphology due to the diverse minerals present therein. The conversion of raw manganese ore into $MnCO_3$ results in most particles with cubical morphology due to the crystal environment of rhombohedral assembly. Such a morphology was also observed by Muralikrishna et. Al. [14]. Similarly, in a study on the synthesis of $MnCO_3$ by ethylene glycol mediated solution method, Zhang and Jia obtained microcubes of $MnCO_3$ particles [11]. Image J software was used to calculate the statistical measures of the particle size from SEM images. The mean length of the $MnCO_3$ particles was found to be 0.308μm with a standard deviation of 0.068.

Figure 6 shows the SEM images of MnO_2 formed at various temperatures. The MnO_2 particles at 500°C retained the cubical shape, while those at 700°C are aggregates of cubical and tubular particles with a rough surface. On the other hand, the majority of

MnO_2 particles at 900°C have transformed into tubular structure with well-defined boundaries and smooth surfaces [31]. Thus, the MnO_2 particles at 500°C can be deemed as cubical MnO_2 polymorph, while the particles at 900°C can be affirmed as tubular MnO_2 polymorph. Such morphologies of MnO_2 particles were also observed by other researchers [15-17]. The MnO_2 particles at 700°C are a mixture of cubical and tubular MnO_2. The mean width of MnO_2 particles at 900°C was 0.266µm with a standard deviation of 0.078.

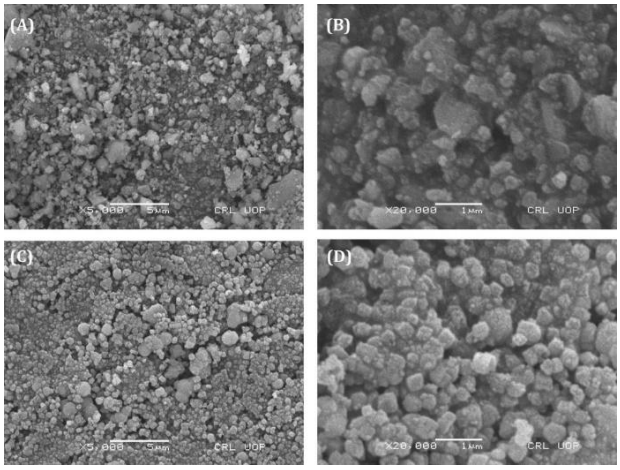

Fig. 5. SEM Images of (A, B) Raw Manganese Ore (C, D) Manganese Carbonate.

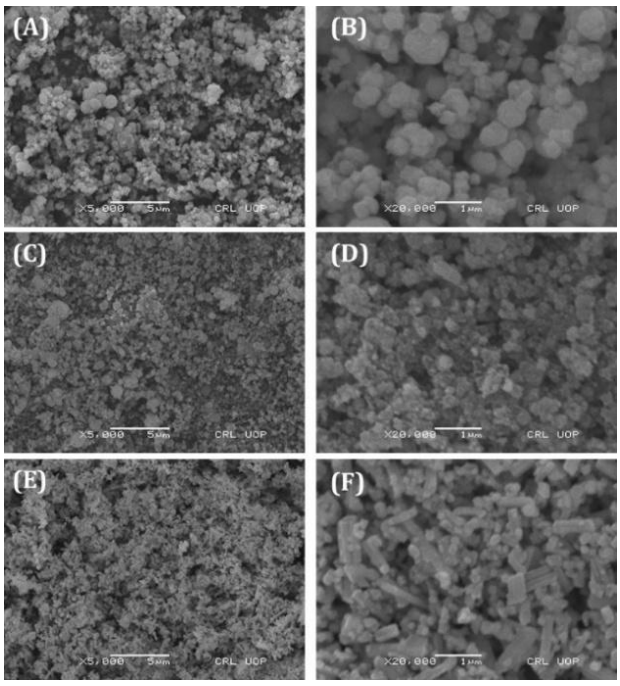

Fig. 6. SEM Images of (A, B) MnO_2 at 500°C (C, D) MnO_2 at 700°C (E, F) MnO_2 at 900°C.

Figure 7 shows the FTIR analysis of raw manganese ore and the synthesized manganese carbonate. The IR spectra of manganese carbonate shows well-resolved peaks at the wavelength of 1388 cm^{-1} and 862 cm^{-1}, which are due to the stretching and planar vibrations of carbonate species, respectively [42]. These peaks confirm the successful synthesis of manganese carbonate. The peaks below 450 cm^{-1} can be assigned to the vibrations of Ca-O bond [43]. The peaks at 455, 474, and 482 cm^{-1} are due to the bending vibrations of Mn-O bond [18, 44], while the peak at 511 cm^{-1} is due to the symmetric vibration of Ca-O bond. The peaks at 1435 cm^{-1} appears due to the bending vibrations of O-H combined with manganese atoms [23, 45]. It can be observed that intensity of bending vibrations of Mn-O bond has significantly reduced in $MnCO_3$ which shows that occurrence of manganese in oxide form has sufficiently abridged. These findings are supported by XRD analysis shown in Figure 5.

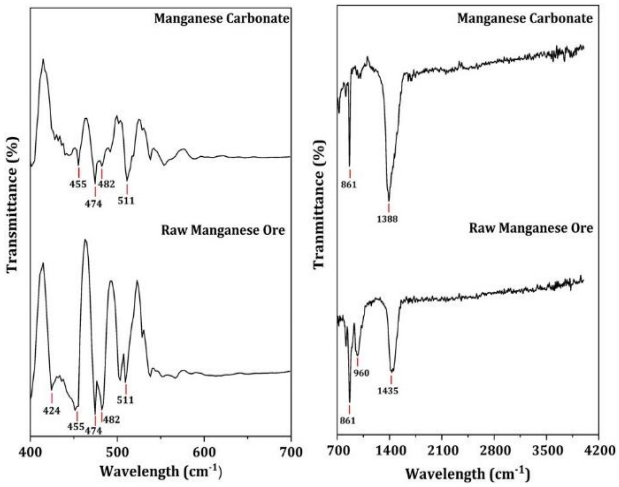

Fig. 7. FTIR Analysis of Raw Manganese Ore & Manganese Carbonate.

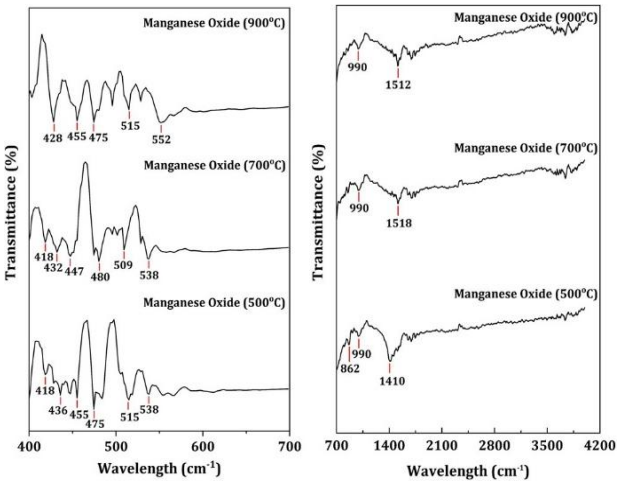

Fig. 8. FTIR Analysis of MnO_2 at Calcination Temperature of 500, 700, and 900°C.

Figure 8 shows the FTIR analysis of manganese oxide synthesized from the calcination of manganese carbonate at 500, 700, and 900°C, respectively. The peaks below 450 cm^{-1} can be assigned to the vibrations of Ca-O bond [43]. The peaks at 447, 455, 475, 480, 538, and 552 cm^{-1} are due to the bending vibrations of Mn-O bond [18, 44]. The peaks at 509 and 515 cm^{-1} are due to the symmetric vibration of Ca-O bond. The peak at 1410 cm^{-1} is due to the vibration of C-O bond [43, 44, 46]. At calcination temperature of 500°C, the peak at 862 cm^{-1} is due to the residual CO_3^{-2}, which diminish with increasing the temperature to 700°C and then 900°C. A small peak at 990 cm^{-1}, which is persistent at all the three calcination temperatures can be attributed to the stretching vibrations of Mn_3O_4 [12, 47]. The peaks at 1410, 1512 and 1518 cm^{-1} occur due to the bending vibrations of O-H combined with manganese atoms [23, 45].

3.1 Yield and Mn content in $MnCO_3$ and MnO_2

Manganese was extracted from the raw ore in the form of manganese chloride using hydrochloric acid as an extractant at temperatures of 50, 70, and 90°C. At each temperature, the extraction process was continued for a time of 3, 6, and 9 hours, respectively. After each extraction, manganese carbonate was precipitated using sodium carbonate as a precipitating agent at room temperature. The percentage yield of manganese carbonate was determined for all experiments. Figure 9 shows the graphical presentation of percent yield of $MnCO_3$ at various temperatures and times, while Figure 10 depicts the percentage of Mn in Manganese Carbonate produced at these temperatures and times. An increase in temperature and time facilitates an efficient extraction of manganese from the raw ore, thereby leading to a comparatively higher yield and purity. It can be observed that the highest yield of 80.52% was obtained at 90°C in a time of 6 hours. The percent Mn content at these parameters was 27.23%. Likewise, at a temperature of 90°C and a time of 6 hours, the $MnCO_3$ yield, and corresponding Mn content was 78.24% and 28.07%, respectively. On the other hand, at a temperature of 70°C and a time of 3 hours, the $MnCO_3$ yield, and corresponding Mn content was 78.10% and 28.54%, respectively. The lowest percent yield was obtained at a temperature of 50°C. The extraction yield of manganese from ore using hydrochloric acid increases with temperature due to enhanced reaction kinetics, greater solubility of manganese chloride, and faster diffusion rates. At higher temperatures, the increased kinetic energy of the molecules overcomes activation energy barriers more effectively, accelerating the reaction rate and enhancing the solubility of $MnCl_2$, which prevents its precipitation and allows for a higher yield. Conversely, at lower temperatures like 50°C, the reaction proceeds more slowly, and solubility limitations may reduce the overall efficiency, resulting in a lower yield.

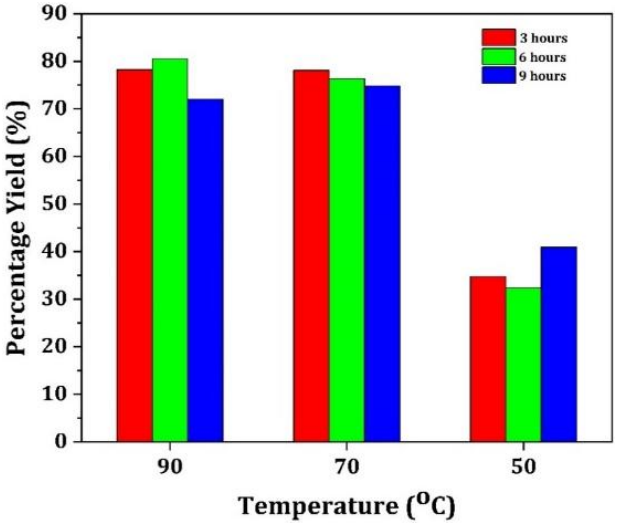

Fig. 9. Percentage Yield of Manganese Carbonate at Various Temperatures and Times.

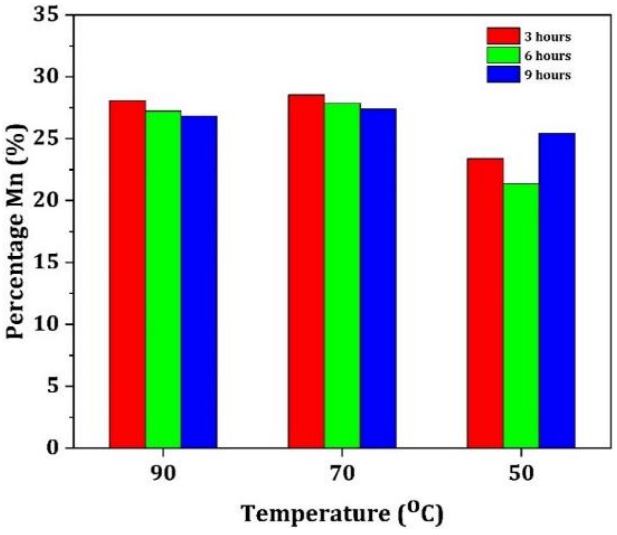

Fig. 10. Mn Percentage in Manganese Carbonate at Various Temperatures and Times.

Keeping in view, the economics of the process and a synergy between the $MnCO_3$ yield, and corresponding Mn content, the recommended optimum conditions for the synthesis of $MnCO_3$ are a temperature of 70°C and time of 3 hours.

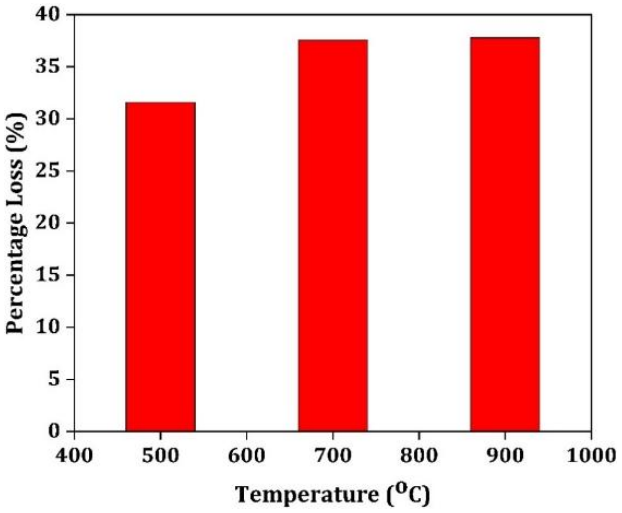

Fig. 11. Percentage Loss in Manganese Carbonate Calcination at Various Temperatures for Synthesis of Manganese Oxide.

Figure 11 shows the loss in weight of $MnCO_3$ during the calcination process for the synthesis of MnO_2 at various temperatures. The percent loss at 500, 700, and 900°C was 31.58, 37.56, and 37.79%, respectively. A higher loss at 700°C shows that most of the carbonates are removed at this temperature. However, for a complete removal of residual carbonates, a further increase in temperature to 900°C is necessary. This argument is supported by EDX analysis shown in Figure 4, where no carbon was detected at 900°C. Similarly, the FTIR analysis shown in Figure 8, also prove the complete removal of carbonates at 900°C.

3.2 Proposed flowsheet for the commercial production of $MnCO_3$ and MnO_2

Figure 12 shows a proposed flowsheet to produce $MnCO_3$ and MnO_2 products on a commercial scale. The raw manganese ore is first crushed in a hammer mill to a size of ½ to 1". The crushed ore is then pulverized in a ball mill to get a particle size of 200 mesh. The ground manganese ore is reacted with hydrochloric acid solution in a leaching reactor at 70°C for 3 hours. As an acidic solution is involved in this reaction, a rubber lined mild steel reactor may be used for this step. The leach solution is then fed to a centrifuge filter where the unreacted solid impurities are filtered to obtain a clear $MnCl_2$ solution. The $MnCl_2$ solution is treated with soda ash solution in a stainless-steel precipitation reactor, which facilitates the precipitation of $MnCO_3$ under mechanical stirring. The resultant $MnCO_3$ slurry is centrifuged to remove the liquid portion and obtain moist $MnCO_3$ solid cake. A rotary dryer is employed to remove the moisture of this cake and obtain dry $MnCO_3$ powder. To obtain MnO_2, the $MnCO_3$ powder is subjected to 900°C in a calcination furnace.

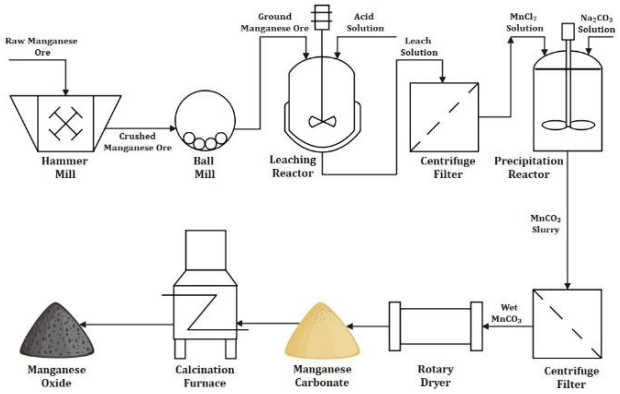

Fig. 12. Flowsheet to produce Manganese Carbonate and Manganese Oxide.

During the production of $MnCO_3$, NaCl is a by-product. To manage and mitigate the presence of NaCl, several strategies can be implemented. First, separating NaCl from the solution can be achieved through evaporation or crystallization processes. By carefully controlling the conditions, NaCl can be precipitated out and removed from the solution, allowing for recovery or safe disposal. Another approach is to use ion exchange or membrane filtration technologies to selectively remove NaCl from the solution before further processing. These methods can help minimize the impact of NaCl and ensure that the solution is suitable for subsequent steps in the process.

3.3 Techno-Economic viability of the developed process

The synthesis of manganese carbonate ($MnCO_3$) from manganese ore using hydrochloric acid (HCl) as an extractant presents a unique and cost-effective alternative to conventional methods that use sulfuric acid (H_2SO_4), nitric acid (HNO_3), organic solvents, ammonia (NH_3), oxalic acid, and cyanide solutions. HCl is widely available and inexpensive, which significantly reduces overall production costs. Unlike sulfuric acid, which is commonly used due to its low cost, organic solvents are less accessible and more expensive. While nitric acid and oxalic acid are effective, their corrosive nature and

environmental hazards make them costly and difficult to handle. Similarly, ammonia and cyanide pose additional safety challenges despite their effectiveness in specific scenarios.

Commercial production of manganese carbonate typically involves sulfuric acid, but recent studies suggest that HCl offers a more cost-effective approach due to its higher reactivity in various extraction processes. Research comparing the extraction of metal oxides from natural clay found that HCl demonstrated superior reactivity compared to both H_2SO_4 and HNO_3, particularly in dissolving alumina silica, which could lead to more efficient extraction processes and reduced operational costs [48]. HCl's efficiency in dissolving various metal phases, including manganese, further supports its use as a preferred extractant in leaching processes [49]. The economic advantage of HCl is underscored by its broader availability and lower cost compared to H_2SO_4, which may be less accessible and more expensive in some regions [50]. HCl's ability to dissolve manganese oxides effectively forms manganese chloride ($MnCl_2$), which can be precipitated as $MnCO_3$. This approach benefits from HCl's strong acidic nature, facilitating rapid breakdown of the ore matrix, resulting in faster processing times and higher purity outputs compared to sulfuric acid, which yields manganese sulfate ($MnSO_4$). Although organic solvents offer excellent selectivity, they require additional steps like phase separation and solvent recovery, adding complexity and cost. Environmentally, HCl has the advantage of generating manageable waste products, primarily chloride ions, as opposed to the sulfate byproducts of sulfuric acid that can contribute to acid mine drainage. Nitric acid poses NO_x emission risks, organic solvents require careful disposal, ammonia can produce complex waste streams, and cyanide is highly toxic, necessitating stringent environmental controls.

To access the economic viability of the developed process over the conventional route, a cost comparison has been made in Table 1 for the manganese extraction using HCl and traditionally used H_2SO_4. The cost estimation involves only major cost components like, raw materials, utilities, heating, and labor costs. Cost estimation reflects the comparison of usage of both electricity and natural gas for heating.

Table 1. Cost comparison of $MnCO_3$ synthesis using HCl and H_2SO_4 as extractants.

Cost Component	Cost for HCl Extraction (USD)	Cost for H_2SO_4 Extraction (USD)
Raw Material Costs		
Manganese Ore (1.39 tons @ USD 36/ton)	50.04	50.04
HCl (33%, 700 kg @ USD 0.108/kg)	75.60	-
H_2SO_4 (98%, 480 kg @ USD 0.216/kg)	-	103.68
Soda Ash (320 kg @ USD 0.45/kg)	144.00	144.00
Utilities Costs (120 kWh @ USD 0.18/kWh)	21.60	21.60
Heating Costs		
Electric Heating (104.5 kWh @ USD 0.18/kWh)	18.81	18.81
Natural Gas Heating (0.357 MMBTU @ USD 15.12/MMBTU)	5.40	5.40
Labor Costs (1 shift @ USD 5.40/shift)	5.40	5.40
Total Cost (Electric Heating)	**315.45**	**343.53**
Total Cost (Natural Gas Heating)	**302.05**	**330.12**

The cost comparison between HCl and H_2SO_4 extraction routes for synthesizing $MnCO_3$ highlights the economic benefits of using HCl. Both methods require the same amount of manganese ore (1.39 tons @ USD 36/ton) and soda ash (320 kg @ USD 0.45/kg). However, HCl extraction incurs a raw material cost of USD 75.60 for 700 kg of HCl (33% concentration), whereas H_2SO_4 extraction requires USD 103.68 for 480 kg of 98% H_2SO_4. This makes the raw material cost for HCl significantly lower. Utilities costs remain constant for both methods at USD 21.60 for 120 kWh of electricity. Heating costs differ based on the energy source: electric heating costs USD 18.81 (104.5 kWh @ USD 0.18/kWh), while natural gas heating is cheaper at USD 5.40 (0.357 MMBTU @ USD 15.12/MMBTU). Labor costs are the same for both routes at USD 5.40 per shift. The total cost of $MnCO_3$ production with electric heating is USD 315.45 for HCl extraction, compared to USD 343.53 for H_2SO_4 extraction. With natural gas heating, the costs are USD 302.05 and USD

330.12, respectively. These results demonstrate that HCl extraction is more cost-effective than H_2SO_4 for $MnCO_3$ synthesis, primarily due to lower raw material costs.

4. CONCLUSION

Manganese ore of district Bajaur, Pakistan, was tested for the synthesis of $MnCO_3$ by using HCl as an extractant, at various temperatures and times. An optimum yield of 78.10% was obtained at a temperature of 70°C and a time of 3 hours. At the same conditions, the maximum content of manganese in $MnCO_3$ was found to be 28.54%. Rhodochrosite was found to be the major mineral phase in the synthesized $MnCO_3$ having a cubical morphology due to the crystal environment of rhombohedral assembly. $MnCO_3$ was then calcined to MnO_2 at elevated temperatures. By increasing temperature from 500 to 900°C, the MnO_2 progressively changed from α-MnO_2 to β-MnO_2 polymorph. However, at each temperature, a mixture of various polymorphs existed, with one crystalline form dominating over the others. $MnCO_3$ and MnO_2 thus prepared can be further tested and applied in various potential areas. The proposed flowsheet for the pilot or commercial production can be used as a basis for industrial viability of the developed products.

REFERNCES

[1] K. Li, J. Chen, J. Peng, M. Omran, and G. Chen, "Efficient improvement for dissociation behavior and thermal decomposition of manganese ore by microwave calcination," *Journal of cleaner production,* vol. 260, p. 121074, 2020.

[2] M. K. Sinha, W. Purcell, and W. A. Van Der Westhuizen, "Recovery of manganese from ferruginous manganese ore using ascorbic acid as reducing agent," *Minerals Engineering,* vol. 154, p. 106406, 2020.

[3] X. Sun, H. Hao, Z. Liu, and F. Zhao, "Insights into the global flow pattern of manganese," *Resources Policy,* vol. 65, p. 101578, 2020.

[4] M. K. Sinha and W. Purcell, "Reducing agents in the leaching of manganese ores: A comprehensive review," *Hydrometallurgy,* vol. 187, pp. 168-186, 2019.

[5] B. Liu, Y. Zhang, M. Lu, Z. Su, G. Li, and T. Jiang, "Extraction and separation of manganese and iron from ferruginous manganese ores: A review," *Minerals Engineering,* vol. 131, pp. 286-303, 2019.

[6] V. Singh, T. Chakraborty, and S. K. Tripathy, "A review of low grade manganese ore upgradation processes," *Mineral Processing and Extractive Metallurgy Review,* vol. 41, no. 6, pp. 417-438, 2020.

[7] Z. You, G. Li, Z. Peng, Y. Zhang, L. Qin, and T. Jiang, "Reductive roasting of iron-rich manganese oxide ore with elemental sulfur for selective manganese extraction," *Journal of Mining and Metallurgy, Section B: Metallurgy,* vol. 53, no. 2, pp. 115-122, 2017.

[8] S. Ali, Y. Iqbal, K. H. Shah, and M. Fahad, "Synthesis and kinetic modeling of manganese carbonate precipitated from manganese sulfate solution," *Chemical Engineering Communications,* vol. 209, no. 1, pp. 96-107, 2022.

[9] S. M. Pourmortazavi, M. Rahimi-Nasrabadi, A. A. Davoudi-Dehaghani, A. Javidan, M. M. Zahedi, and S. S. Hajimirsadeghi, "Statistical optimization of experimental parameters for synthesis of manganese carbonate and manganese oxide nanoparticles," *Materials Research Bulletin,* vol. 47, no. 4, pp. 1045-1050, 2012.

[10] Y. Lu, R. Gao, J. Song, W. Li, and G. Hu, "Synthesis of Manganese Carbonate Templates with Different Morphologies and Their Application in Preparing Hollow MoS2 Micro/Nanostructures for Photocatalysis," *Journal of Nanoscience and Nanotechnology,* vol. 20, no. 4, pp. 2239-2246, 2020.

[11] Y.-X. Zhang and Y. Jia, "Fluoride adsorption on manganese carbonate: ion-exchange based on the surface carbonate-like groups and hydroxyl groups," *Journal of colloid and interface science,* vol. 510, pp. 407-417, 2018.

[12] I. A. Reyes *et al.*, "Kinetics of the thermal decomposition of rhodochrosite," *Minerals,* vol. 11, no. 1, p. 34, 2020.

[13] C. M. M. Yannick *et al.*, "Manganese Dioxide (MnO2) Gaining by Calcination of Manganese Carbonate (MnCO3) Precipitated from Cobalt Removal Solutions," *Open Journal of Applied Sciences,* vol. 12, no. 04, pp. 598-613, 2022.

[14] S. Muralikrishna, B. Kishore, H. Nagabhushana, D. Suresh, S. Sharma, and G. Nagaraju, "One pot green synthesis of MnCO 3–rGO composite hybrid superstructure: application to lithium ion battery and biosensor," *New Journal of Chemistry,* vol. 41, no. 21, pp. 12854-12865, 2017.

[15] X. Huang, D. Lv, H. Yue, A. Attia, and Y. Yang, "Controllable synthesis of α-and β-MnO2: cationic effect on hydrothermal crystallization," *Nanotechnology,* vol. 19, no. 22, p. 225606, 2008.

[16] S. Srither, A. Karthik, D. Murugesan, S. Arunmetha, M. Selvam, and V. Rajendran, "Electrochemical capacitor study of spherical

MnO2 nanoparticles utilizing neutral electrolytes," *Front. Nanosci. Nanotechnol,* vol. 1, pp. 13-20, 2015.

[17] H. Wang *et al.*, "Toluene conversion by using different morphology Mno2 catalyst," *Aerosol and Air Quality Research,* vol. 22, no. 2, p. 210365, 2022.

[18] Y. Khan, S. K. Durrani, M. Mehmood, and M. R. Khan, "Mild hydrothermal synthesis of γ-MnO2 nanostructures and their phase transformation to α-MnO2 nanowires," *Journal of Materials Research,* vol. 26, no. 17, pp. 2268-2275, 2011.

[19] L. Feng *et al.*, "MnO 2 prepared by hydrothermal method and electrochemical performance as anode for lithium-ion battery," *Nanoscale research letters,* vol. 9, pp. 1-8, 2014.

[20] W. Wang *et al.*, "Synthesis of MnO2 nanoparticles with different morphologies and application for improving the fire safety of epoxy," *Composites Part A: Applied Science and Manufacturing,* vol. 95, pp. 173-182, 2017.

[21] E. D. Rus, G. D. Moon, J. Bai, D. A. Steingart, and C. K. Erdonmez, "Electrochemical behavior of electrolytic manganese dioxide in aqueous KOH and LiOH solutions: a comparative study," *Journal of The Electrochemical Society,* vol. 163, no. 3, p. A356, 2015.

[22] J. Chen *et al.*, "Electrochemical properties of MnO2 nanorods as anode materials for lithium ion batteries," *Electrochimica Acta,* vol. 142, pp. 152-156, 2014.

[23] V. Sannasi and K. Subbian, "Influence of Moringa oleifera gum on two polymorphs synthesis of MnO2 and evaluation of the pseudo-capacitance activity," *Journal of Materials Science: Materials in Electronics,* vol. 31, no. 19, pp. 17120-17132, 2020.

[24] Y. Iqbal, "JPMS Conference Issue, Materials 2010," 2010.

[25] A. Kazmi and S. Abbas, "Metallogeny and mineral deposits of Pakistan," *Islamabad: Orient Petroleum Inc,* pp. 88-150, 2001.

[26] S. Naseem, "Genesis of manganese ore deposits Of Lasbela area, Balochistan Pakistan," 1996.

[27] R. Bilqees, F. Haqqani, and F. Khan, "Mineralogical characterization and evaluation of manganese ore from Bajaur Agency, Khyber Pakhtunkwa, Pakistan," *Journal of Himalayan Earth Sciences,* vol. 47, no. 1, p. 1, 2014.

[28] F. U. Khan, M. Riaz, A. Yamin, R. Bilquees, and N. Muhammad, "Beneficiation Studies of Bajaur Manganese Ore by Different Processing Techniques: Benefication of Manganese Ore," *Biological Sciences-PJSIR,* vol. 53, no. 6, pp. 298-302, 2010.

[29] W. U. Rehman, A. U. Rehman, F. Khan, A. Muhammad, and M. Younas, "Studies on beneficiation of manganese ore through high intensity magnetic separator," *Advances in Sciences and Engineering,* vol. 12, no. 1, pp. 21-27, 2020.

[30] D. Amalia and A. Azhari, "Potency of making the chemical manganese dioxide (CMD) from East Nusa Tenggara pyrolusite," *Indonesian Mining Journal,* vol. 19, no. 2, pp. 79-87, 2016.

[31] Z. Y. Leong and H. Y. Yang, "A study of MnO2 with different crystalline forms for pseudocapacitive desalination," *ACS applied materials & interfaces,* vol. 11, no. 14, pp. 13176-13184, 2019.

[32] K. Nimako, A. Dwumfour, K. Mensah, P. Koshy, and J. Dankwah, "Calcination behaviour of Nsuta rhodochrosite ore in the presence and absence of end-of-life high density polyethylene," *Ghana Mining Journal,* vol. 20, no. 2, pp. 27-35, 2020.

[33] T. Tămaş, F. Kristály, and L. Barbu-Tudoran, "Mineralogy of Iza Cave (Rodnei Mountains, N. Romania)," *International Journal of Speleology,* vol. 40, no. 2, p. 10, 2011.

[34] P. Sahoo and A. Venkatesh, "'Indicator'carbonaceous phyllite/graphitic schist in the Archean Kundarkocha gold deposit, Singhbhum orogenic belt, eastern India: Implications for gold mineralization vis-a-vis organic matter," *Journal of Earth System Science,* vol. 123, pp. 1693-1703, 2014.

[35] S. Yuan, W. Zhou, Y. Han, and Y. Li, "Efficient enrichment of low-grade refractory rhodochrosite by preconcentration-neutral suspension roasting-magnetic separation process," *Powder Technology,* vol. 361, pp. 529-539, 2020.

[36] S. S. Al-Jaroudi, A. Ul-Hamid, A.-R. I. Mohammed, and S. Saner, "Use of X-ray powder diffraction for quantitative analysis of carbonate rock reservoir samples," *Powder Technology,* vol. 175, no. 3, pp. 115-121, 2007.

[37] S. E. Kaczmarek *et al.*, "Dolomite, very-high magnesium calcite, and microbes: implications for the microbial model of dolomitization," in *Characterization and Modeling of Carbonates–Mountjoy Symposium*, 2017, vol. 1, pp. 7-20.

[38] T. R. Reddy, K. Thyagarajan, O. A. Montero, S. R. L. Reddy, and T. Endo, "X-Ray Diffraction, Electron Paramagnetic Resonance and Optical Absorption Study of Bauxite," *Journal of Minerals and Materials Characterization and Engineering,* vol. 2014, 2014.

[39] A. Shoppert, D. Valeev, K. Alekseev, and I. Loginova, "Enhanced Precipitation of Gibbsite from Sodium Aluminate Solution by Adding Agglomerated Active Al (OH) 3 Seed," *Metals,* vol. 13, no. 2, p. 193, 2023.

[40] C. Zhou *et al.*, "Magnetic and thermodynamic properties of α, β, γ and δ-MnO 2," *New Journal of Chemistry,* vol. 42, no. 11, pp. 8400-8407, 2018.

[41] M. Musil, B. Choi, and A. Tsutsumi, "Morphology and Electrochemical Properties of α-, β-, γ-, and δ-MnO2 Synthesized by Redox Method," *Journal of the Electrochemical Society,* vol. 162, no. 10, p. A2058, 2015.

[42] M. Pudukudy and Z. Yaakob, "Synthesis, characterization, and photocatalytic performance of mesoporous α-Mn2O3 microspheres prepared via a precipitation route," *Journal of Nanoparticles,* vol. 2016, 2016.

[43] M. Galvan-Ruiz, L. Banos, and M. E. Rodriguez-Garcia, "Lime characterization as a food additive," *Sensing and Instrumentation for Food Quality and Safety,* vol. 1, pp. 169-175, 2007.

[44] S. Ashoka, P. Chithaiah, C. N. Tharamani, and G. T. Chandrappa, "Synthesis and characterisation of microstructural α-Mn2O3 materials," *Journal of Experimental Nanoscience,* vol. 5, no. 4, pp. 285-293, 2010.

[45] M. Perachiselvi, M. S. Bagavathy, J. J. Samraj, E. Pushpalaksmi, and G. Annadurai, "Synthesis and characterization of Mn3O4 nanoparticles for biological studies," *Appl. Ecol. Environ. Sci.,* vol. 8, no. 5, pp. 273-277, 2020.

[46] L. Habte, N. Shiferaw, D. Mulatu, T. Thenepalli, R. Chilakala, and J. W. Ahn, "Synthesis of nano-calcium oxide from waste eggshell by sol-gel method," *Sustainability,* vol. 11, no. 11, p. 3196, 2019.

[47] K. Devaraj *et al.*, "Study on effectiveness of activated calcium oxide in pilot plant biodiesel production," *Journal of cleaner production,* vol. 225, pp. 18-26, 2019.

[48] S. Side, "The Effect of Acid Treatment on Metal Oxide Content of South Sulawesi Natural Clay," *Indonesian Journal of Fundamental Sciences,* vol. 8, no. 2, p. 118, 2022.

[49] S. Niessen, B. Ouddane, and J. Fischer, "Effects of Acid Volatile Sulfides on the Use of Hydrochloric Acid for Determining Solid-Phase Associations of Mercury in Sediments," *Environmental Science & Technology,* vol. 34, no. 9, pp. 1871-1876, 2000.

[50] P. Numluk and A. Chaisena, "Sulfuric Acid and Ammonium Sulfate Leaching of Alumina From Lampang Clay," *Journal of Chemistry,* vol. 9, no. 3, pp. 1364-1372, 2011.